Front. Optoelectron. 2021, 14(2): 170–186
https://doi.org/10.1007/s12200-021-1201-9

REVIEW ARTICLE

Metalenses: from design principles to functional applications

Xiao FU[1], Haowen LIANG (✉)[1,2], Juntao Li[1]

1 State Key Laboratory of Optoelectronic Materials and Technologies, School of Physics, Sun Yat-sen University, Guangzhou 510275, China
2 Southern Marine Science and Engineering Guangdong Laboratory (Zhuhai), Zhuhai 519080, China

Abstract Lens is a basic optical element that is widely used in daily life, such as in cameras, glasses, and microscopes. Conventional lenses are designed based on the classical refractive optics, which results in inevitable imaging aberrations, such as chromatic aberration, spherical aberration and coma. To solve these problems, conventional imaging systems impose multiple curved lenses with different thicknesses and materials to eliminate these aberrations. As a unique photonic technology, metasurfaces can accurately manipulate the wavefront of light to produce fascinating and peculiar optical phenomena, which has stimulated researchers' extensive interests in the field of planar optics. Starting from the introduction of phase modulation methods, this review summarizes the design principles and characteristics of metalenses. Although the imaging quality of existing metalenses is not necessarily better than that of conventional lenses, the multi-dimensional and multi-degree-of-freedom control of metasurfaces provides metalenses with novel functions that are extremely challenging or impossible to achieve with conventional lenses.

Keywords metalens, achromatic aberration, phase modulation, wavefront manipulation

1 Introduction

Free control of light has always been the dream and pursuit of optics community, which not only has important scientific significance, but also has a wide range of applications in the fields of information, industry, and energy. Since 1968, the establishment of negative refraction theory provides a new concept for free control of electromagnetic waves [1–5]. The observation of negative refraction phenomena in well-designed metamaterials has experimentally demonstrated electromagnetic wave manipulation [6–8]. The electromagnetic response of metamaterials can be designed according to engineering requirements, which realizes a series of electromagnetic wave control phenomena that cannot be achieved in natural materials, including super lensing [9–12], transformation optics [13–15], perfect absorption [16–19], polarization deflection [20,21], and phase modulation [22,23].

The planar-structured metamaterial, also known as "metasurface," has the advantages of easy fabrication and low transmission losses. Moreover, it can maintain a remarkable electromagnetic control ability. This material is gradually attracting more attention than the three-dimensional structure. Eventually, the fundamental principles of light manipulation in metasurfaces deviate from those in metamaterials; thus, metasurfaces become an independent branch in artificial materials research [24–27]. In a pioneering work on metasurface, the periodically arranged V-shaped antennas act as sub-wavelength resonance units to modify the phase response of a certain frequency, which results in an abrupt phase change [28]. Under external light stimulation, the metasurface loads the "phase jump" on the radiated electromagnetic waves, which can achieve artificially designed intensity and phase distribution of electromagnetic waves to manipulate the wavefronts.

Lenses are one of the most widely used components in the optical field. For hundreds of years, people have devoted themselves into the development of superb skills to polish the lenses to achieve control of light based on refractive optics [29]. Metalens is a diffractive lens designed on the basis of metasurface, which creates a new research direction of lens fabrication by engraving nanostructured patterns on a thin film. In recent years, numerous studies have significantly improved the performance and functions of metalens by designing and analyzing the optical response of nanostructures [30–33]. Currently, some properties of metalenses can reach or even exceed those of conventional optical lenses. Compared with conventional diffractive optical lens, which is also a planar optical element, metalens can independently and simultaneously control the effects of electric and magnetic

Received January 4, 2021; accepted February 21, 2021

E-mail: lianghw26@mail.sysu.edu.cn

fields at a sub-wavelength scale, which results in the manipulation of phase, amplitude, and polarization. Therefore, metalenses have greater potential than conventional diffractive lenses.

Since metalens is one of the important applications of metasurfaces, in this review article, we first present three phase modulation methods of metasurfaces before introducing the design principles of metalenses. Furthermore, we discuss the main challenges of metalens design. Then, we summarize the research progress on metalenses and finally discuss the functional applications and future development trends of metalenses.

2 Design principles of metalenses

From the perspective of phase modulation mechanism, metasurfaces can be categorized into three: resonance phase metasurfaces (Figs. 1(a) and 1(b)), geometric phase metasurfaces (Figs. 1(c) and 1(d)), and propagation phase metasurfaces (Figs. 1(e) and 1(f)).

In the early days, most studies were focused on the resonance phase modulation [28,37–52]. By changing the structure of meta-atoms, the resonance frequency is shifted, which leads to a sudden change in the phase at a certain frequency. Resonance phase metasurfaces can be used to control the deflection [47], focusing [38,49], and polarization conversion [42,45,52] of electromagnetic waves. However, resonance phase modulation has limitations. Initially, metal antennas were used to form the resonance phase metasurface. It is clear that metal materials can build high-performance reflection- and transmission-type metasurfaces for long wavelengths. However, metal resonance phase metasurfaces suffer the problem of high ohmic loss for the visible. Thus, the transmission efficiency of resonance metasurfaces is always low at this wavelength range. Since the phase jump comes from the resonance of the structures, this leads to high absorption and limited working bandwidth of resonance phase metasurfaces. Moreover, it requires precise design and processing of structures with negligible differences in size to accurately control the phase.

To solve this kind of difficulties, geometric phase (also called Pancharatnam–Berry phase) modulation was proposed [34,53–74]. This modulation method generates a sudden change in the phase of reflected or transmitted waves by changing the rotation angle of the nanostructures, thereby achieves free control of the phase gradient or distribution. The complexity of designing and processing metasurfaces is greatly reduced due to the concept of geometric phase modulation. Geometric phase metasurfaces make full use of their degrees of freedom to manipulate a large number of spin-dependent electromagnetic wave phenomena, such as abnormal deflection or refraction [68,70,71], holographic imaging [61,64,65,67,73,74], and special beam generation [53,69,72]. Generally, the emergence of geometric phase metasurfaces provides us with more freedom for electromagnetic wave manipulation.

The propagation phase metasurfaces manipulate the phase through the optical path difference generated during the propagation of electromagnetic waves. Assuming that an electromagnetic wave with a wavelength of λ propagates a certain distance d in a homogeneous medium with a refractive index n, the accumulated propagation phase of electromagnetic waves can be expressed as

$$\phi = nk_0 d, \tag{1}$$

where $k_0 = 2\pi/\lambda$ is the free space wave vector. According to Eq. (1), the thickness d and refractive index n of an optical element are two parameters that can effectively adjust the propagation phase. For planar optical elements, without increasing the thickness d, the phase design can be achieved by spatially varying the equivalent refractive index n. In addition, if the equivalent refractive index n is sufficiently large, the thickness of the device can be effectively reduced. The commonly used methods for the construction of propagation phase metasurfaces can be divided into two categories: one is based on the theory of waveguide optics, and the other is based on the theory of equivalent refractive index of the medium. The difference between these two methods lies in the way of adjusting the refractive index. The former adopts the characteristic that the propagation constant of the waveguiding mode changes with the fill factor of the meta-atom [75–78]. The latter uses the difference in the refractive index of two or more media (usually one is a high refractive index medium) in the unit structure to achieve the phase modulation of electromagnetic waves [35,36,79–82].

Three phase modulation principles of metasurfaces were introduced above. In addition, there are some metasurface devices that are not based on a single phase modulation method but integrate two or more types of phase manipulations. Taking V-shaped antennas as an example, the design principle combines the modulation of resonance phase and geometric phase [28,83–86]. Figure 2(a) presents an eight-step phase manipulation, which consists of two sets of sub-wavelength structures rotated 90° along the z axis [28]. The first four V-antennas adjust the resonance phase by tuning the length of the rods and angle between the two rods; the last four V-antennas realize the additional geometric phase of π by rotating the first four 90°. This combined modulation is widely used in optical components, such as metalenses [85,86,88–90], wave plates [83], and deflectors [84].

The metasurfaces formed by nano-fins with rectangular [87,91–95] or elliptical [96,97] cross-section can essentially be understood as the simultaneous manipulation of propagation phase and geometric phase by varying the dimensions and rotation angle of the nano-fins. As

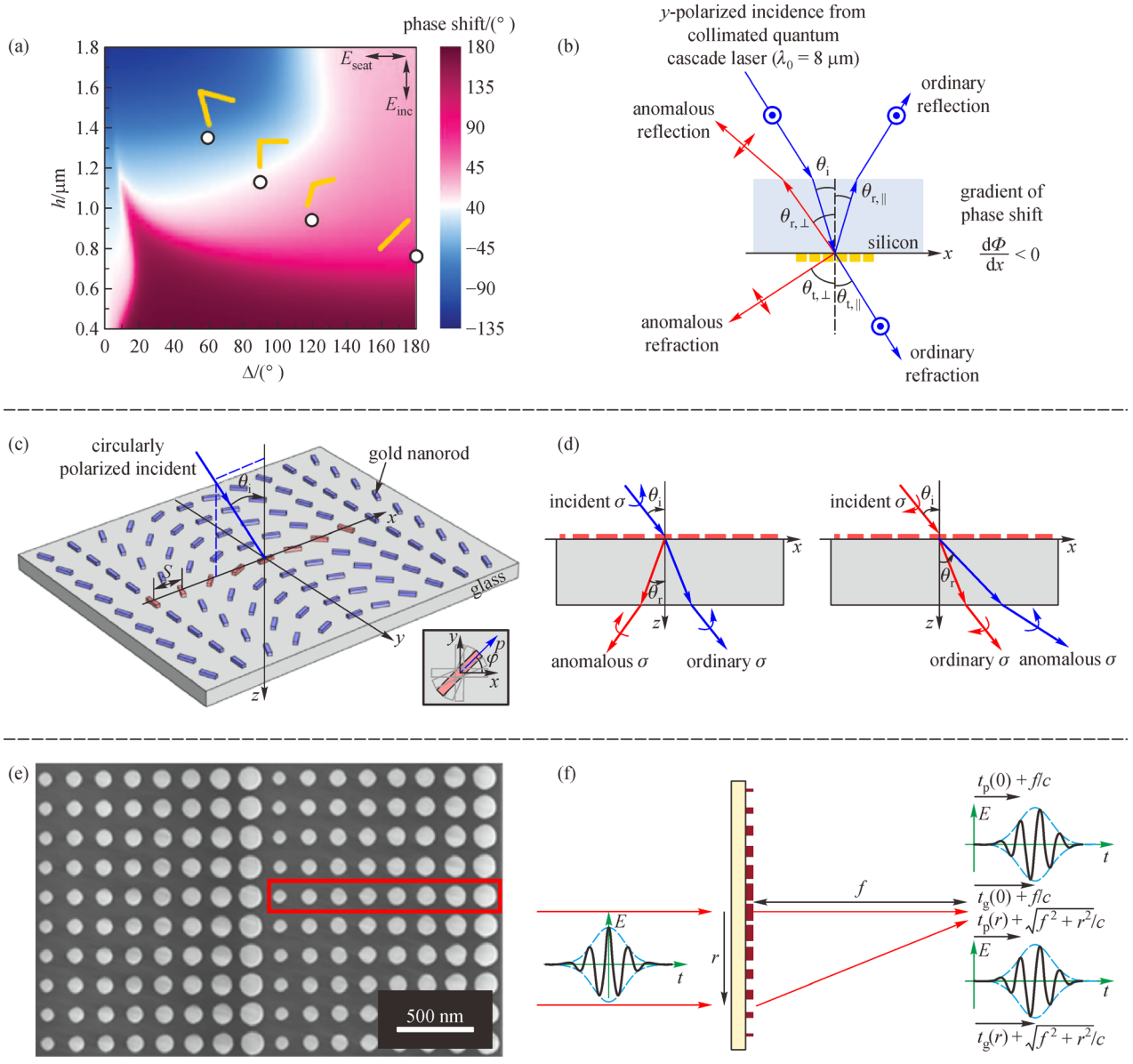

Fig. 1 Schematic diagram of three phase modulation methods, i.e., resonance phase modulation ((a) and (b)), geometric phase modulation ((c) and (d)), and propagation phase modulation ((e) and (f)). (a) Simulated phase shift of the scattered light for V-antennas with various length h and angle between the rods Δ. (b) Schematic diagram of ordinary and anomalous reflection and refraction for y-polarized excitation. (c) Schematic diagram of a representative meta-atom array considered as model in the simulation. Bottom right: excitation of dipole moment when illuminating one meta-atom. (d) Schematic diagram of ordinary and anomalous refraction when illuminated with left- and right-circularly polarized light, respectively. (e) Side-view scanning electron microscope (SEM) image of a propagation phase-modulated metasurface. An array of nanopillars is indicated by red rectangle. (f) Schematic diagram of focusing a light pulse to the focal distance of a propagation phase-modulated metalens. The time-dependent electric field plots demonstrate that the light passing through the different parts of the metalens requires equal phase delay to arrive at the focal point without dispersion. (a) and (b) Reproduced with permission from Ref. [28]. (c) and (d) Reproduced with permission from Ref. [34]. (e) Reproduced with permission from Ref. [35]. (f) Reproduced with permission from Ref. [36]

mentioned above, the change in dimensions can modify the propagation phase of each meta-atom; the rotation of nano-fins can achieve geometric phase regulation (see Fig. 2(b)). The combination of geometric and propagation phase modulation can be applied to metasurface devices, such as polarization controllers and detectors [87,93–96], beam deflectors [98], and multifocal metalenses [91,92,97].

The metasurface that can focus and image was named as a “metalens” [54,68,76,85,86,99–101]. To realize the function of a diffraction-limited lens, the phase distribution $\varphi(r)$ of the metalens is expressed as

$$\varphi(r) = -\frac{\omega_d}{c}\left(\sqrt{r^2 + f^2} - f\right), \tag{2}$$

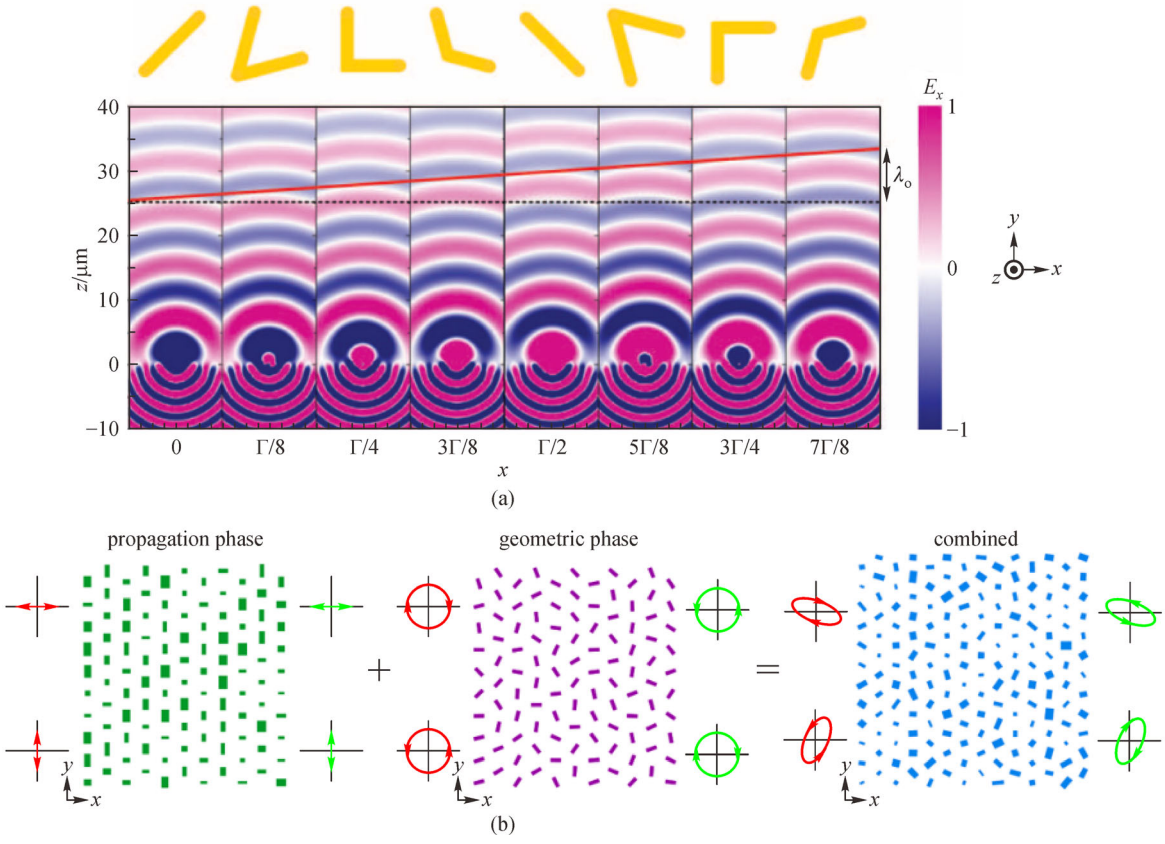

Fig. 2 (a) Top: schematic diagram of meta-atoms. Bottom: finite difference time-domain (FDTD) simulations of the scattered electric field of the periodic array composed of individual antennas shown above. (b) Schematic diagram of the combination of propagation and geometric phases. (a) Reproduced with permission from Ref. [28]. (b) Reproduced with permission from Ref. [87]

where ω_d is the design frequency, c is the speed of light, r is the distance of each nanostructure to the center of the metalens, and f is the focal length.

The first metalens that is comparable to commercial lenses was fabricated by Capasso's group in 2016 [68]. In this work, high aspect ratio titanium dioxide (TiO_2) meta-atoms were used to design and fabricate metalenses with a diameter $D=2$ mm, focal length $f=0.725$ mm, and numerical aperture NA = 0.8 (Fig. 3). It can resolve sub-wavelength separated nanostructures and has a magnification of up to 170×. The diffraction-limited focusing of the metalens was demonstrated at 405, 532, and 660 nm wavelengths with corresponding efficiencies of 86%, 73%, and 66%.

3 Innovation in full-color imaging

The research on metalenses has aroused widespread concern in both scientific and industrial communities. People are considering whether metalenses can obtain novel sub-wavelength focusing imaging and replace conventional optical lenses, with the purpose of compact and efficient imaging. However, there is the chromatic aberration problem, i.e., inability to perform full-color imaging by metalens. Chromatic aberration is a serious defect for lens imaging, which refers to the slight difference in focal lengths of light at different wavelengths. The traditional method of chromatic aberration correction is to stack multiple lenses. However, this will cause problems such as bulkiness and complex integration.

Multi-wavelength achromatic metasurface devices that compensate the phase dispersion are demonstrated [36,97,102,103]. For example, the metasurface designed by Khorasaninejad et al. is based on low-loss dielectric resonators associated with different transverse electric and magnetic modes to compensate the propagation phase difference between discrete wavelengths [102]. First, a metasurface that can deflect incident light to the same angle at three wavelengths (1330, 1550, 1800 nm) was demonstrated. Furthermore, a two-dimensional multi-wavelength achromatic metalens was designed with a numerical aperture of 0.05 and focal length of 7.5 mm (Fig. 4 (a)).

In recent years, various scientific research teams have begun to explore the combination of resonance phase modulation and geometric phase modulation to design continuous broadband achromatic metalens [88]. With this

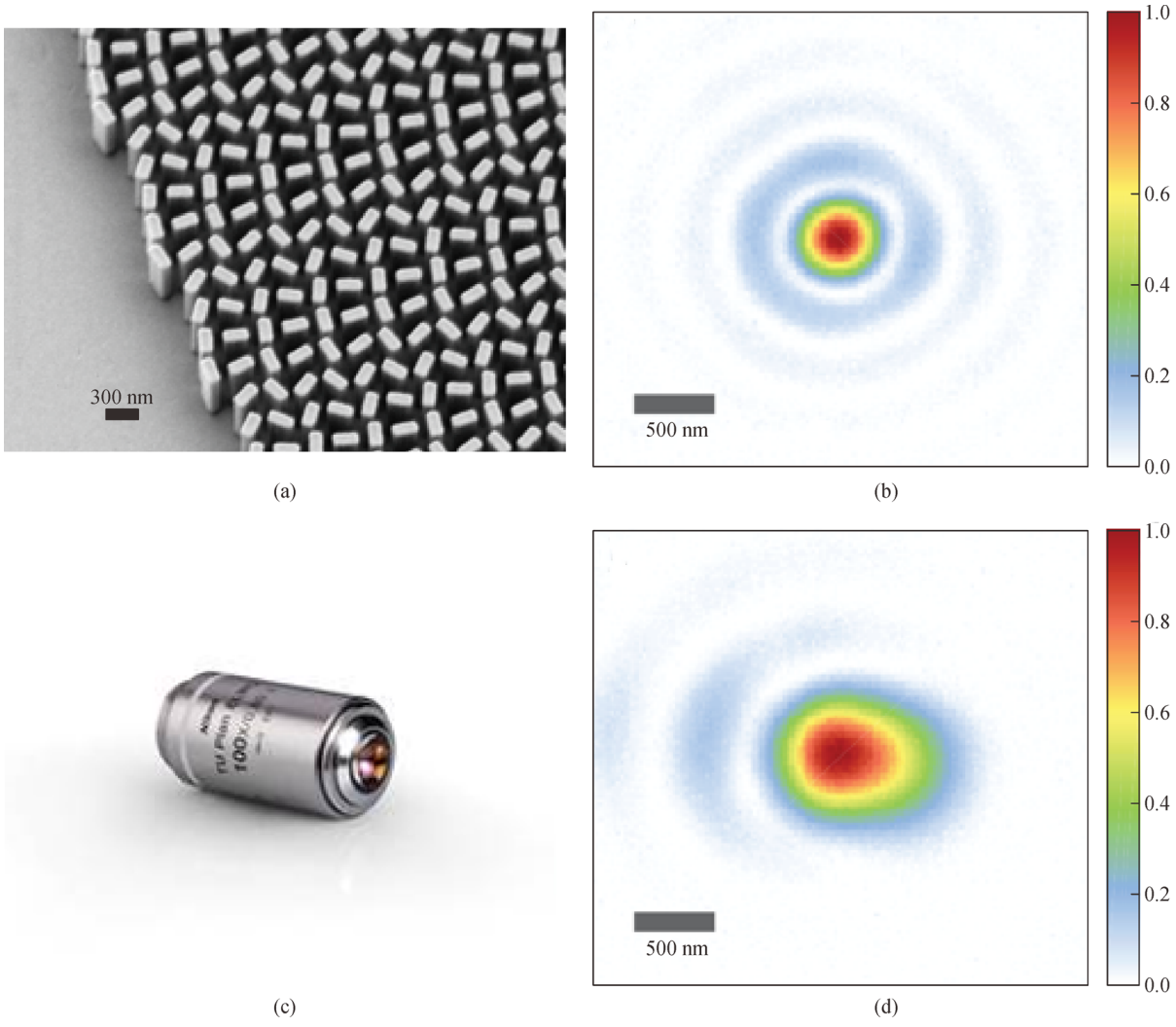

Fig. 3 (a) SEM micrograph of the fabricated metalens. Wavelength = 532 nm. (c) Picture of the Nikon objective lens (100× CFI60, NA = 0.8). (b) and (d) Measured focal spot intensity profiles of the metalens in (a) and the commercial objective lens in (c) at the wavelength of 532 nm. (a), (b), and (d) Reproduced with permission from Ref. [68]. (c) From the Nikon website

method, integrated metal resonators are utilized to build up high-order resonance in a broad range of wavelengths to compensate the wavelength-dependent geometric phase delay generated from rotating the resonance elements (Fig. 4(b)). This approach successfully eliminated the chromatic aberration of metalens over a continuous wavelength range of 1200–1680 nm [88]. Soon after, they used the same method to achieve achromatic imaging in the visible light region using gallium nitride (GaN) nanopillars [106].

Similar work has also been done by using TiO_2 dielectric pillars to achieve achromatic imaging in the visible light region [89] (Fig. 4(c)). This study expanded the fundamental equation of metalens design (Eq. (3)) as a Taylor series near a design frequency and determined the influence of higher-order derivative terms in Eq. (4), which are the relative group delay and group delay dispersion, on the chromatic aberration of metalens. It also clearly demonstrated the simultaneously control of the phase, group delay, and group delay dispersion of light, thereby realizing a transmissive broadband achromatic metalens.

$$\varphi(r,\omega) = -\frac{\omega}{c}(\sqrt{r^2+f^2}-f), \tag{3}$$

$$\varphi(r,\omega) = \varphi(r,\omega_{\rm d}) + \frac{\partial\varphi(r,\omega)}{\partial\omega}|_{\omega=\omega_{\rm d}}(\omega-\omega_{\rm d}) + \frac{\partial^2\varphi(r,\omega)}{2\partial\omega^2}|_{\omega=\omega_{\rm d}}(\omega-\omega_{\rm d})^2+\cdots. \tag{4}$$

The phase compensation of a single antenna has an upper limit. With an increase in the designed numerical aperture and metalens size, the required phase compensation becomes larger. However, due to the ceiling of physical principle and limitation of the manufacturing

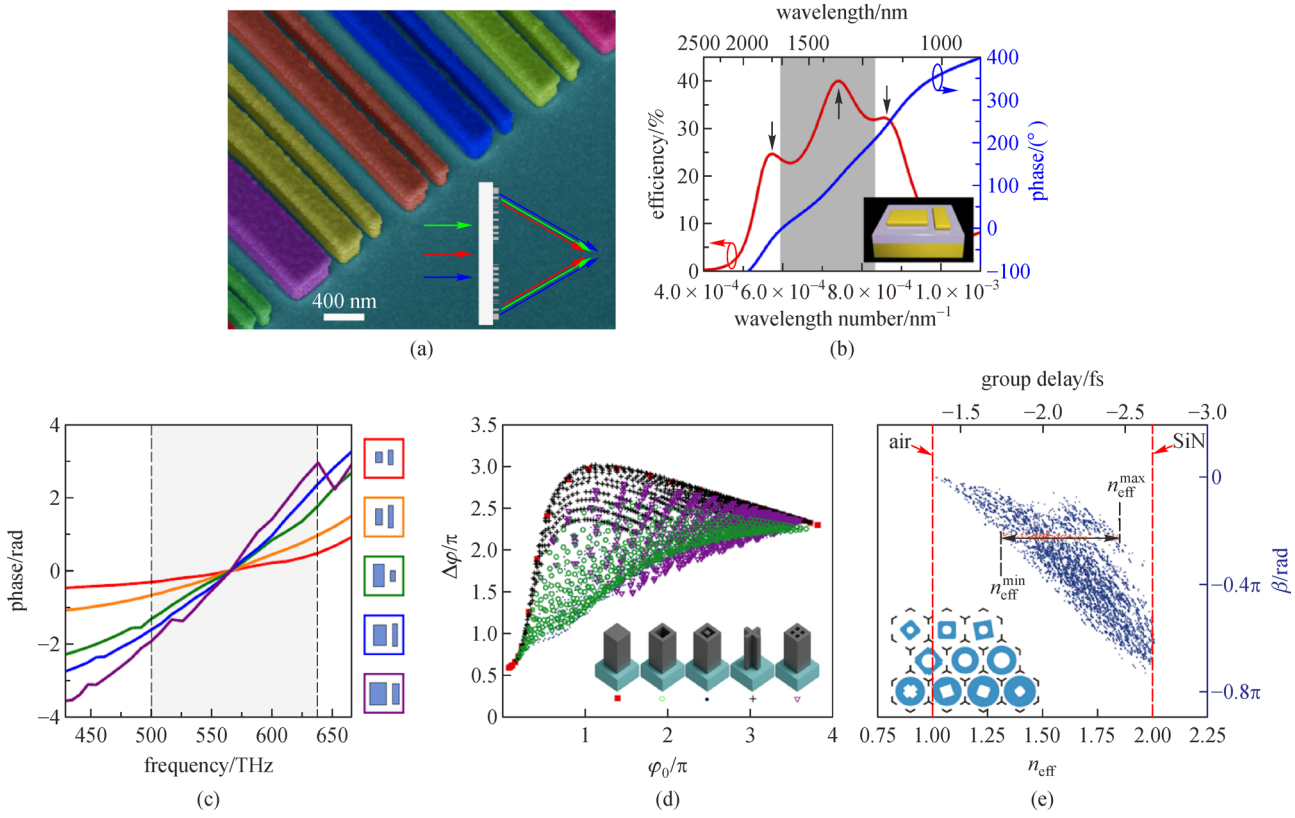

Fig. 4 Multi-wavelength achromatic metalenses. (a) False colored SEM image of achromatic metalens. Inset: schematic side view of metalens designed to focus three different wavelengths into the same focal plane. (b) Schematic diagram of one integrated-resonant unit cell of the broadband achromatic metalens for the incident wavelengths varying from 1200 to 1680 nm. (c) Phase spectra for five different elements schematically shown on the right. The shaded region indicates the design bandwidth of 120 nm. (d) Calculated phase φ_0 and dispersion $\Delta\varphi = \dfrac{\mathrm{d}\varphi}{\mathrm{d}\omega}\Delta\omega$ for the meta-atom library schematically shown in the inset. (e) Calculated n_{eff} for all designed meta-atoms. The meta-atoms schematically shown in the inset are chosen to compose the broadband achromatic metalens by selecting the maximum Δn_{eff}. (a) Reproduced with permission from Ref. [102]. (b) Reproduced with permission from Ref. [88]. (c) Reproduced with permission from Ref. [89]. (d) Reproduced with permission from Ref. [104]. (e) Reproduced with permission from Ref. [105]

process and material selection, such a large phase compensation cannot be satisfied. Therefore, this method suffers from the limitation of small numerical aperture, and the single metalens imaging technique is still a long way from commercialization. Researchers then put forward the concept of "metalens array", which exploits an array of metalenses to image different aspects of the image on the corresponding pixels of the CCD camera; then, the entire image is reconstructed via image stitching [107].

The design principle of a broadband achromatic metalens demonstrated in Shrestha's work divided the spectral phase profile into two parts: initial phase φ_0 and phase dispersion $\Delta\varphi$ [104] (Fig. 4(d)).

$$\varphi(r,\omega) = \varphi_0(r) + \frac{\mathrm{d}\varphi}{\mathrm{d}\omega}(r)(\omega-\omega_0). \tag{5}$$

The physical nature of achromatic aberration is analyzed using the concept of effective refractive index n_{eff} [104]. Then, the phase profile (Eq. (5)) is expressed in a more general form for a continuous wavelength range.

$$\varphi_0(r) = \frac{\omega_0}{c} n_{\text{eff}}(\omega_0) H, \tag{6}$$

and

$$\begin{aligned}\Delta\varphi(r) &= \frac{\mathrm{d}\varphi}{\mathrm{d}\omega}(r)(\omega-\omega_0)\\ &= \frac{H}{c}\left(n_{\text{eff}}(\omega)\omega - n_{\text{eff}}(\omega_0)\omega_0\right),\end{aligned} \tag{7}$$

where H is the height of meta-atoms.

According to Eq. (7), if the operational wavelength range is fixed, increasing the height of the meta-atoms and/or choosing a material with higher refractive index could enlarge the phase dispersion. Thus, the high aspect ratio fabrication technique and material refractive index limit the design radius of metalenses. Fan et al. gave similar relationship between effective refractive index and group delay [105] (Fig. 4(e)).

In fact, these three methods of constructing broadband

achromatic metalens (i.e., integrated-resonance unit elements, group delay, and effective refractive index) share the same design principle: making use of the spectral degrees of freedom in the metasurface phase profiles and the geometric degrees of freedom in the meta-atoms. Most of the existing broadband achromatic metalenses [30,31,88,89,102,104–116] working from the visible light region to the microwave region are based on such a design principle.

However, the design of achromatic metalens with simultaneously large size, large numerical aperture, and wide band is still a long way to go in metalens technology. The main reason is that there are inherent constraints between the various parameters of the metalens under the government of diffractive optics. Shrestha et al. derived an expression to describe the relationship between design parameters of a hyperbolic broadband achromatic metalens (Eq. (4) in Ref. [104]).

$$R_{\max} \leqslant \frac{\Delta \Phi' c}{\Delta\omega\left(\frac{1}{\mathrm{NA}} - \sqrt{\frac{1}{\mathrm{NA}^2} - 1}\right)}. \tag{8}$$

Here, $R_{\max}$ is the maximum radius, $\Delta\omega$ is the operational bandwidth, and NA is the numerical aperture of the designed broadband achromatic metalens. $\Delta\Phi'$ defines the range of phase dispersion in the meta-atom design. Equation (8) demonstrates the trade-offs that the broadband achromatic metalens with simultaneously large radius and high numerical aperture requires extremely large phase dispersion. This equation is only valid when describing a single-layer broadband achromatic metalens with hyperbolic phase profile, which is designed based on the unit-cell method. For other phase profiles, this trade-off relationship remains, but the specific mathematical expression varies.

Thus, for broadband achromatic metalenses (Table 1), assuming the radius of the designed metalens is $R_{\max}$, the minimum $\Delta\Phi'$ of each metalens is calculated based on Eq. (8). It demonstrates that the improvements of size and NA require larger range of phase dispersion in the meta-atom design. In addition, by forcing operational wavelengths toward visible range and by extending the bandwidth, $\Delta\omega$ increases, which leads to smaller size and/or NA of achromatic metalens with limited phase dispersion range. It is worth noting that the metasurface device listed in the third row of Table 1 is not a single broadband achromatic metalens, and its phase profile is not hyperbolic [90]. Therefore, the calculation of $\Delta\Phi'$ using Eq. (8) is not applicable here.

A high-performance broadband achromatic metalens requires simultaneously large $R_{\max}$, NA, and $\Delta\omega$, which means that more complicated meta-atoms, higher aspect ratio, and perhaps multilayer design are involved to cover the enormous phase dispersion. However, at the same time, the difficulty of the design and processing also inevitably increases. Currently, expanding the range of phase dispersion is one of the main research focuses of broadband achromatic metalens.

To make a metalens comparable to a commercial lens, the focusing efficiency of metalens should be at least 90%.

Table 1 Summary of broadband achromatic metalenses

radius/μm	NA	wavelength range/nm	$\Delta\omega$/Hz	minimum $\Delta\Phi'/\pi$	focal length/μm	material	focusing efficiency	comment	Ref.
27.775	0.268	1200–1680	7.14×10^{13}	0.29	100	Au	12%	reflection scheme	[88]
220	0.02	470–670	1.91×10^{14}	0.44	63	TiO_2	20%		[89]
750	0.075	475–700	2.03×10^{14}	N/A*	9960	TiO_2	35%	refractive lens and metacorrector with air gap	[90]
50	0.24	1300–1650	4.90×10^{13}	0.32	200	amorphous silicon	20%–58%		[104]
50	0.24	1200–1650	6.82×10^{13}	0.44	200				
100	0.13	1200–1650	6.82×10^{13}	0.47	800				
50	0.88	1200–1400	3.57×10^{13}	1.13	30		N/A		
25	0.106	400–660	2.95×10^{14}	0.42	235	GaN	40%		[106]
16.67	0.36	1310–1550	3.55×10^{13}	0.12	38	Si	50.07%–55.53%	theoretical work	[109]
13.2	0.2	460–700	2.24×10^{14}	0.32	67	TiO_2	30%		[110]
7	0.086	430–780	3.13×10^{14}	0.10	81.5	SiN	36%–55%		[105]
32	0.81	1470–1590	1.54×10^{13}	0.27	22.95	Si	21%–27%	theoretical work	[112]
	0.1			0.08	60		43%–78%		
6.25	0.9	450–700	2.38×10^{14}	0.99	3	TiO_2	13%–32%	theoretical work	[113]
	0.99			1.37	0.9		23%–36%		

Note: *This device is a hybrid lens consisting of a metacorrector and a spherical lens. Thus, the hyperbolic phase profile is not applicable here.

However, the focusing efficiency of broadband achromatic metalenses does not exceed 60% (see Table 1). Even the theoretical simulation result generated from an infinite library of meta-atoms cannot reach 80% [113]. This gap is caused by principles, materials, and fabrication techniques. In theory, a focusing efficiency of 100% will be possible when the periodic sequence of meta-atoms in the broadband achromatic metalens design includes all possible solutions [113]. The mismatch between the ideal fields and the ideal periodic-diffraction-order fields results in the fundamental efficiency losses, regardless of the imperfection of material selection and manufacturing process. Higher diffraction orders appeared at the abrupt discontinuities shown in the inset of Fig. 5 are introduced due to the increase in unit-cell period (N_d= 1 when unit-cell period is smaller than the wavelength). Figure 5 indicates that for a relatively large metalens ($R = 50\lambda$), there will be a significant efficiency loss at high numerical apertures. The five curves for each diffraction order correspond to different values of unit-cell period normalized to wavelength. Therefore, the values of radius, NA, operational bandwidth, and focusing efficiency of broadband achromatic metalenses are limited (see Table 1).

Another important aspect, which has to be considered for real applications of metalenses, is the fabrication process. Compared with the time-consuming and costly hand-polishing manufacturing processes of high-performance conventional lenses performed by experienced craftsmen [29], metalenses have advantages over conventional lenses in terms of manufacturing process, benefitting from the matured nanoscale processing techniques, such as UV lithography, electron beam lithography (EBL), atomic layer deposition (ALD), nano-imprinting, and plasma etching [117]. However, improving the yield and efficiency of production for the metalenses with complicated nanostructures is still challenging. In summary, broadband achromatic metalenses still have a long way to go before commercialization due to the limitations in performance.

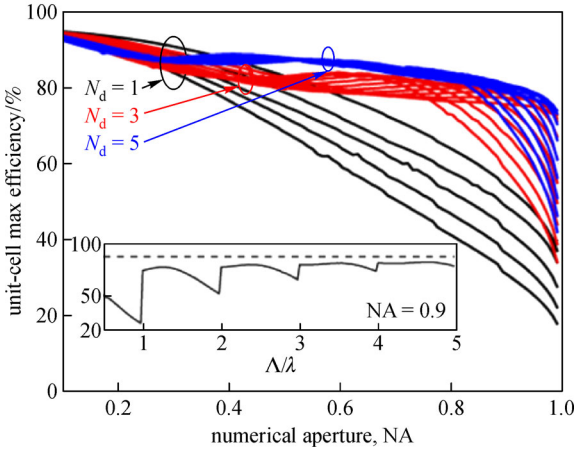

Fig. 5 Simulated maximum focusing efficiency of a metalens designed by the unit-cell approach for diffraction order N_d is equal to 1 (black), 3 (red), and 5 (blue), respectively. Inset: maximum efficiency as a function of unit-cell periods Λ divided by the wavelength λ. Reproduced with permission from Ref. [113]

4 Functional applications of metalenses

Replacing traditional lenses is simply making use of the phase modulation of metalenses; yet, the outstanding features of metalenses lie in the manipulation of multiple optical parameters in the whole light field, including phase, polarization, chromatic control, and correlation. The use of such optical features is able to achieve special functionalities that cannot be achieved with conventional optics or on a single thin element. Such functional abilities allow metalenses to improve tunable lens systems, ultrahigh-resolution microscopes, phase gradient microscopes, and tomography systems.

4.1 Flat high-resolution focusing and imaging

High-resolution imaging faces two problems. The first is that the imaging system is complex and heavy, and the other is that the resolution is limited by the diffraction limit. Metalenses, which have the advantages of flatness, high degree of freedom, high integration, and multi-field adjustment, can simultaneously solve the above mentioned problems.

Conventional sub-wavelength resolution imaging lenses are bulky and expensive. The development of metalens makes it possible to flatten and lighten the high-resolution imaging system. The first proposed metalens fabricated by Khorasaninejad et al. with a high NA of 0.80 achieved sub-wavelength resolution at the visible wavelength range [68] (Fig. 6(a)). In another work, a metalens based on crystalline silicon reached a high NA of 0.98 in air with a focal spot size (full width at half maximum, FWHM) of 274 nm and a focusing efficiency of 67% under 532 nm wavelength illumination [100] (Fig. 6(b)). Uniquely, this metalens can be directly immersed into oil to experimentally achieve an ultrahigh NA of 1.48, which further narrows down the FWHM of the focal spot to 211 nm [100] (Fig. 6(c)).

There are also other approaches that can realize ultrahigh-resolution focusing and imaging beyond the diffraction limit. For example, geometric phase metasurface can be designed as a super-oscillatory filter due to its independence from wavelength [119]. With the application of super-oscillatory metasurface filter, the imaging system achieved a resolution of about 0.64 times that of the Rayleigh criterion over the whole visible wavelength range [119] (Fig. 6(d)). Zuo et al. took advantage of the controllable polarization of the metasurface to convert the incident linearly polarized light into focused radially polarized light [118] (Fig. 6(e)). With the enhancement of the longitudinal polarization component by the circular

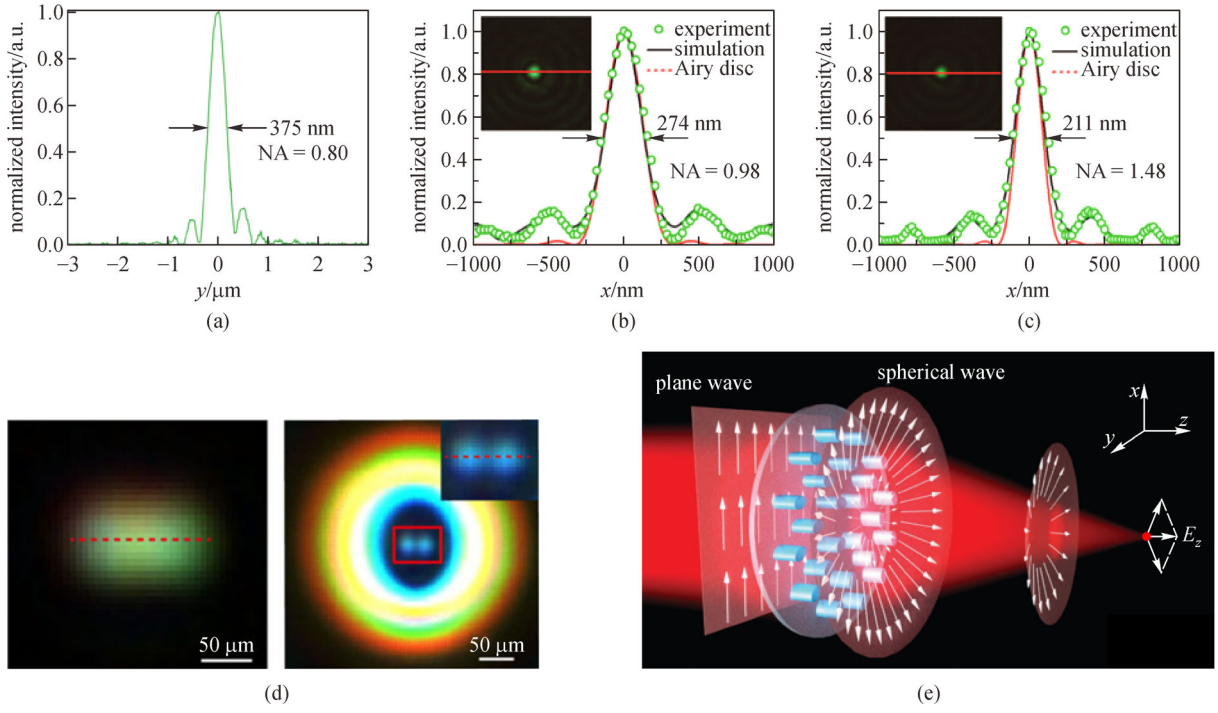

Fig. 6 High-resolution metalenses. Vertical cuts of the measured focal spot intensity profile of the metalens designed at 532 nm with (a) NA = 0.80, (b) NA = 0.98, and (c) NA = 1.48 in immersion oil, respectively. (d) Diffraction-limited image (left) and super-oscillatory image with the application of metasurface filter (right). (e) Schematic illustration of the designed resolution-enhanced metalens described in Ref. [118]. (a) Reproduced with permission from Ref. [68]. (b) and (c) Reproduced with permission from Ref. [100]. (d) Reproduced with permission from Ref. [119]. (e) Reproduced with permission from Ref. [118]

high-pass aperture, the focal spot is confirmed to be much smaller than the diffraction limit. Furthermore, with the elimination of the transversal polarization component by an extra phase distribution, the low-frequency part at the center of this metalens is filtered out, which further shrinks the focal spot [118].

4.2 Multifocal metalenses

Multifocal lens has a wide range of applications in imaging and beam scanning, which is usually achieved by changing the distance between multiple optical elements. The use of conventional optical refractive elements makes the entire multifocal lens system bulky, slow in adjustment, and limited in variation range. The emergence of metalens enables light and thin optical elements to have precisely designed phase profiles, making compact multifocal lens systems possible.

Using Jones matrix calculations, the diffraction orders and phase profiles of a bi-layer geometric phase metalens were analyzed. Then, it is demonstrated that the bi-layer geometric phase metalens split the incident circularly polarized beam into different helicities and then focused them to different focal points under controllable intensity and focal length [120] (Fig. 7(a)). The combination of two values of phase and two values of amplitude forms four orders of polarization.

Apart from using multiple layers of metasurfaces, multifocal function can also be accomplished by using only one metalens. A polarization-dependent metalens with two focal points along the longitudinal direction was designed by Tian et al. with the combination of geometric phase modulation and propagation phase modulation [92]. More importantly, the relative intensity of the two focal points and the separation distance between the two focal points can be arbitrarily manipulated (Fig. 7(b)). A similar design [122], which was proposed by Khorasaninejad et al., could simultaneously form two images with opposite helicities along the lateral direction in the same field of view (Fig. 7(c)). This compact chiral imager can detect chiral optical properties in the visible spectrum without the addition of polarizers or diffusors.

Researchers have also used different rectangular hydrogenated amorphous silicon nano-posts to create a twofold polarization-selective metalens [121]. By simultaneously tailoring the linear polarization of the incident and transmitted light, three focal points located on different focal planes along the longitudinal direction are successfully obtained (Fig. 7(d)). Zang et al. have proposed a multifocal metalens based on geometric phase modulation using silicon pillars with different spatial orientations [123]. It has been experimentally demonstrated that both

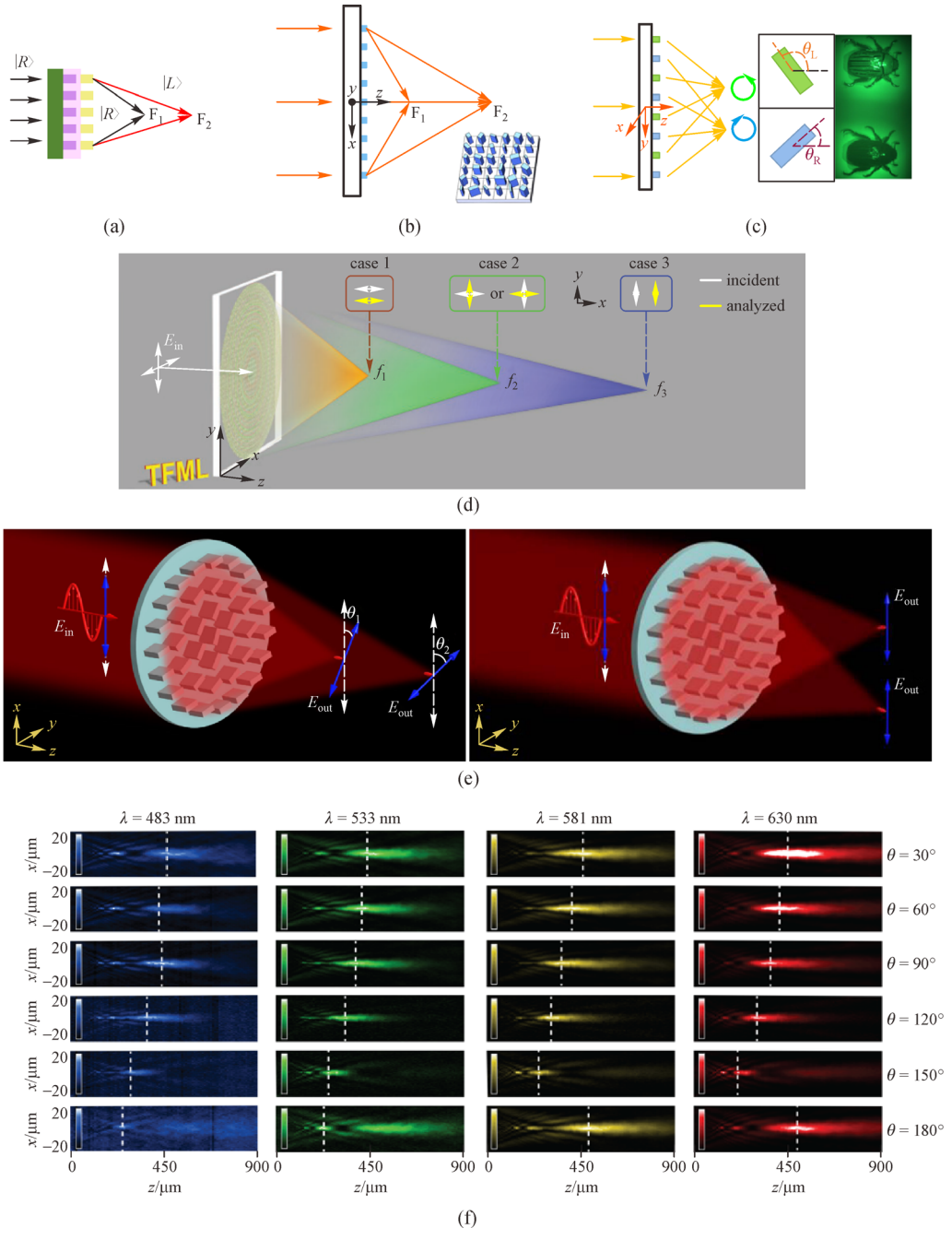

Fig. 7 (a) Schematic diagram of the working principle of the bifocal lens proposed in Ref. [120]. (b) Schematic diagram of the working principle of the designed bifocal metalens [92]. Bottom right: top view of the designed metalens consisting of nano-fins with same height but different cross sizes and orientations. (c) Schematic diagram of the multispectral chiral imaging metalens where the left-circularly polarized (LCP) light and right-circularly polarized (RCP) light from the same object are focused into two spots. Spiral arrows indicate helicity of the incident light. Blue and green nano-fins (top view) impart the phase profile required to focus RCP light and LCP light, respectively. The upper half of the image is formed by focusing the LCP light reflected from the beetle, whereas the lower half of the image is formed by focusing the RCP light reflected from the beetle. (d) Schematic diagram of the twofold polarization-selective metalens indicated in Ref. [121]. (e) Left: under the illumination of linearly polarized THz waves, two longitudinally distributed polarization-rotated focal points are demonstrated. Right: under the illumination of *x*-polarized THz waves, two transversely distributed focal points are demonstrated. (f) Measured point spread function of the achromatic varifocal metalens by rotating the polarization of linearly polarized input light of visible wavelengths. (a) Reproduced with permission from Ref. [120]. (b) Reproduced with permission from Ref. [92]. (c) Reproduced with permission from Ref. [122]. (d) Reproduced with permission from Ref. [121]. (e) Reproduced with permission from Ref. [123]. (f) Reproduced with permission from Ref. [124]

longitudinal and transversal multifocal focusing can be realized by pre-designed polarization rotation (Fig. 7(e)). Aiello et al. have reported a varifocal metalens that can continuously change the focal length from 220 to 550 μm by rotating the polarization of linearly polarized incident light [124] (Fig. 7(f)). The principle of this design is based on the use of asymmetric TiO_2 nanostructures to induce polarization-dependent optical responses. The uniqueness of these polarization-dependent multifocal metalenses may open a new opportunity for imaging, tomography, holography, and optical data processing.

Polarization-sensitive multifocal metalenses offer the possibility of adding novel functions, which will contribute to the development of compact multifunctional imaging systems.

A tunable multifocal metalens system was experimentally demonstrated by changing the distance between a converging metalens and a diverging metalens using microelectromechanical system (MEMS) [125]. Moreover, the researchers also verified through simulation that if a third metalens was prepared on the back of the glass substrate, a simple objective lens with magnification function can be realized (Fig. 8(a)). This system has a potential to compose a compact scanning microscope for 3D imaging [125]. Yilmaz et al. have proposed a rotationally adjustable metalens doublet inspired by Moiré lenses [126] (Fig. 8(b)). By rotating two dielectric metasurfaces with opposite phase distributions, the system can modify the focal length in a wide range. This polarization-insensitive multifocal Moiré metalens can be applied to generate tunable multifocal, single-focal, and non-focal phenomena [126]. Another rotationally tunable metalens doublet proposed by Wei et al. could not only vary focal length on the positive direction, but also cover a large range of negative focal length (Fig. 8(c)) [127].

Polarization-insensitive multifocal metalenses can adapt to all types of incident light without reducing the image quality. Some achromatic metalenses mentioned in Section 3 are also polarization-insensitive [77,90,105,110,128]. This design gets rid of the constraints of incident light polarization on the metalenses and improves the tolerance of metalenses in different illumination environments.

4.3 Other functional imaging

A compact quantitative phase gradient microscope (QPGM) was proposed based on two integrated metasurfaces [129]. Its principle, which is demonstrated in Fig. 9(a), is to capture three differential interference contrast (DIC) images in one shot and then generate a quantitative phase gradient image. This vertically integrated functional metalens microscope has been verified by experimentally capturing phase gradient images of transparent samples [129]. The quantitative phase imaging (QPI) of transparent samples plays a vital role in biomedical research, and the emergence of metalenses makes these systems miniaturized, which can be applied to point-of-care diagnostics and *in vivo* imaging.

Two orthogonal polarizations were used in another study (shown in Fig. 9(b)) to independently adjust different light fields (lens focus and spiral phase), which allows to realize switching between bright-field imaging and spiral phase

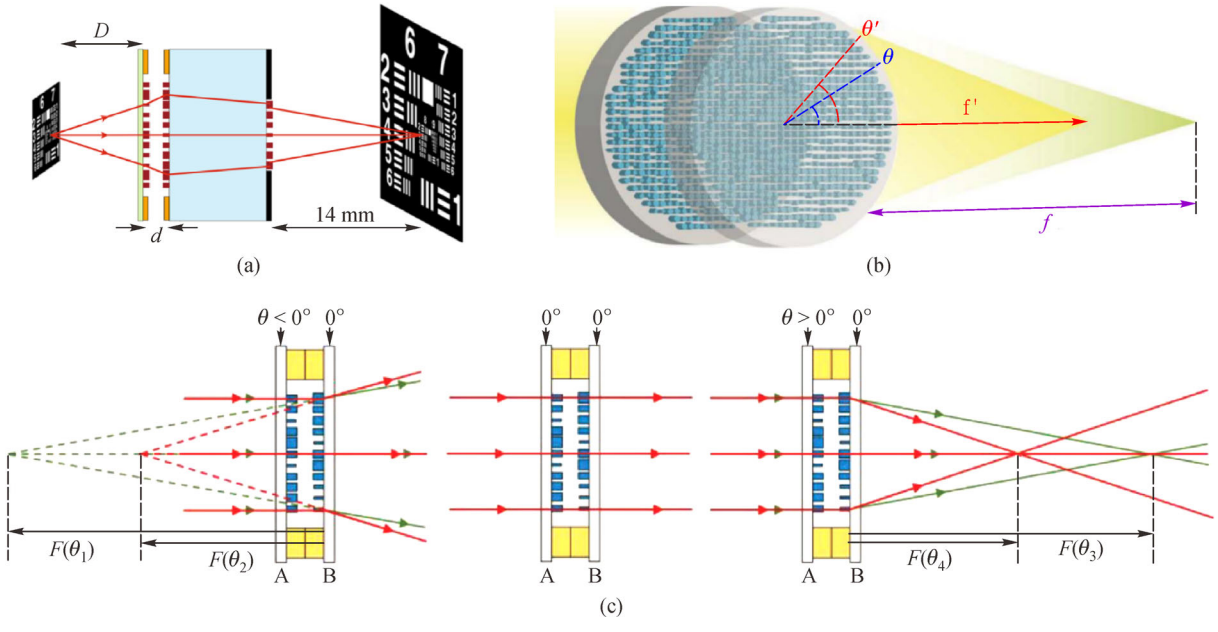

Fig. 8 (a) Schematic diagram of the MEMS-assisted metasurface triplet operating as a compact focus tunable microscope. (b) Schematic diagram of the rotationally tunable multifocal Moiré metalens. (c) Schematic diagrams of the rotationally tunable metalens doublet showing negative focal length variation (left), no focus (middle), and positive focal length variation (right). (a) Reproduced with permission from Ref. [125]. (b) Reproduced with permission from Ref. [126]. (c) Reproduced with permission from Ref. [127]

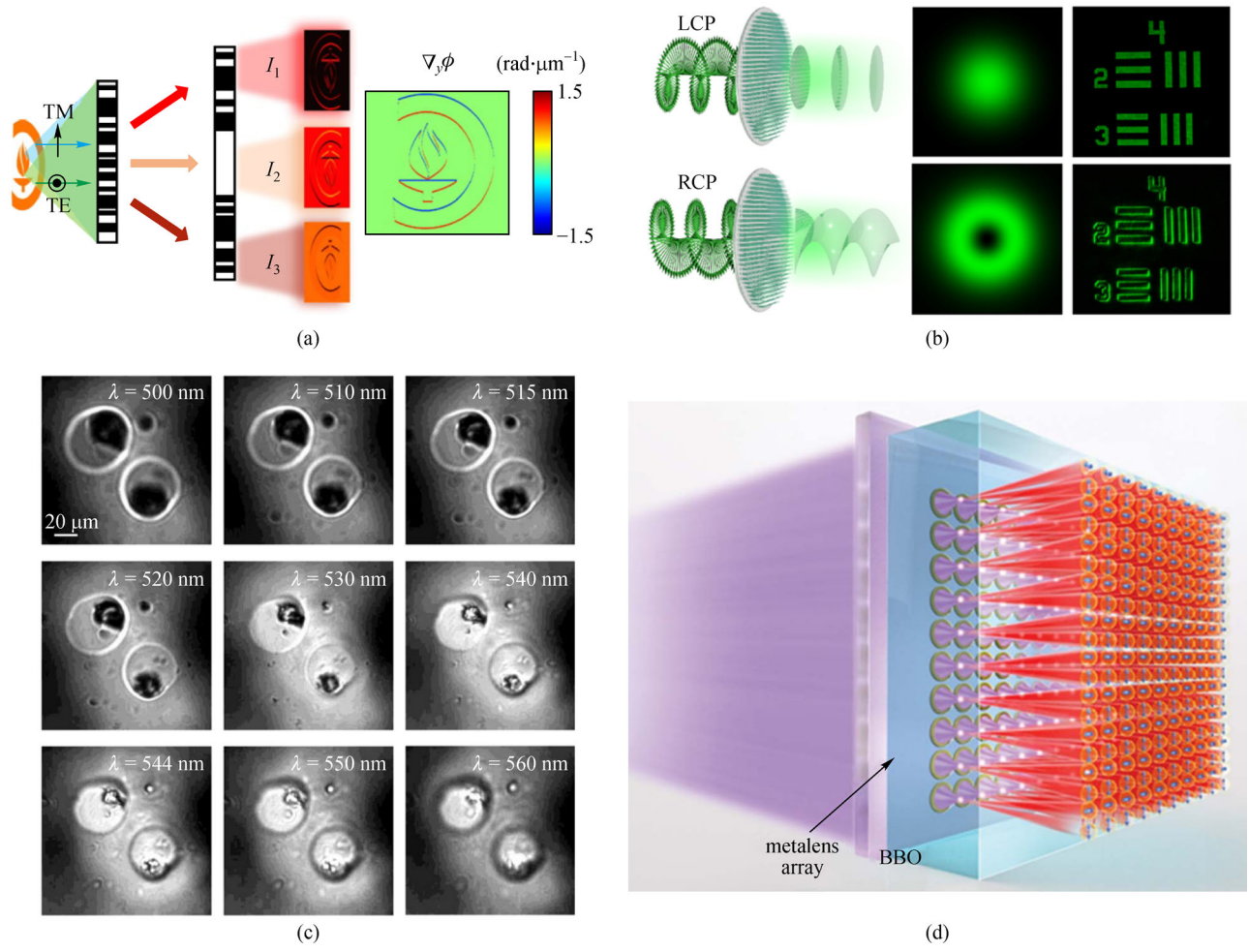

Fig. 9 (a) Left-hand side: schematic diagram of the principle of QPGM. Right-hand side: phase gradient image (PGI) formed by combining three DIC images (I_1, I_2, and I_3). (b) LCP incident on the metasurface results in an output beam with Gaussian intensity distribution and a bright-field image. RCP incident on the same metasurface results in an output beam with donut-shaped intensity distribution and a spiral phase contrast image. (c) Microscopic spectral tomography images of frog egg cells with aplanatic metalens at different wavelengths. (d) Schematic diagram of the metalens-array-based quantum source. (a) Reproduced with permission from Ref. [129]. (b) Reproduced with permission from Ref. [130]. (c) Reproduced with permission from Ref. [131]. (d) Reproduced with permission from Ref. [132]

contrast imaging [130]. This multifunctional imaging can also be applied to other light fields to achieve active control of imaging.

The previous section mentioned that researchers have made a lot of efforts to eliminate the chromatic aberration of metalenses. However, Chen et al. made full use of large diffractive dispersion characteristics of metalenses to design a spectral imaging system to achieve spectral focus tuning and optical zooming in the visible light spectrum [131] (Fig. 9(c)). Tomographic images of two microscopic frog egg cells were pictured by this metalens with excellent depth-of-field (DOF) features [131].

Owing to the advantages of fast speed, long coherence time, and large information capacity of photon, quantum optical systems are one of the most significant physical systems in the field of quantum information processing. However, the generation of high-fidelity, large-dimensional, and multiphoton entangled quantum light sources is still challenging. Li et al. utilized GaN metalens array to encode the spontaneous parameter process of nonlinear crystals for generating and controlling complex quantum source [132]. This approach not only increases the dimensionality of quantum entanglement, but also allows coherent control of multiple photons (Fig. 9(d)). This compact, stable, and controllable quantum source has the potential to provide an ideal platform for the development of advanced on-chip quantum photonic information processing.

5 Conclusions and outlook

The processing technology and application of metalenses have been rapidly developed in recent years. In this paper, we summarized the design principles of metalenses, the approaches of broadband achromatic metalenses for full-color imaging, and the functional applications of metalenses.

Following the development of metasurface, the material of metalenses have been developed from metallic to transparent dielectric materials for manipulating light in a broader wavelength range from ultraviolet to infrared; the optical field modulation methods have been expanded from single-phase modulation approach to combining the manipulation methods of various optical parameters for realizing specific functions; the structures of metalenses have been complicated from single layer to multiple layers for achieving multiple functions; the operational principles of metalens have been exploited from static switching the optical properties of light to dynamic tuning the electromagnetic waves for a series of continuous manipulation.

Metalenses can realize flexible design of phase, amplitude, and polarization in the sub-wavelength scale and have the advantages of planarization and low loss. In many specific application circumstances, the introduction of metalens can effectively promote the integration, improve the reliability, and expand the functions of optical systems. We believe that the future development of metalens may head to two completely different directions: simple structure but pursuing extreme performance and complex design but integrating multiple functions. Therefore, rather than completely replacing conventional optical lenses, metalenses have a brighter future to functionalize the optical systems, and manipulate electromagnetic wave at sub-wavelength scale under specific application occasions.

Acknowledgements This work was supported by the National Key R&D Program of China (No. 2020YFC2007102), the National Natural Science Foundation of China (Grant No. 12074444), and Guangdong Basic and Applied Basic Research Foundation (No. 2020A1515011184), Innovation Group Project of Southern Marine Science and Engineering Guangdong Laboratory (Zhuhai).

References

1. Veselago V G. The electrodynamics of substances with simultaneously negative values of ε and μ. Soviet Physics Uspekhi, 1968, 10(4): 509–514
2. Pendry J B, Holden A J, Stewart W J, Youngs I. Extremely low frequency plasmons in metallic mesostructures. Physical Review Letters, 1996, 76(25): 4773–4776
3. Pendry J B, Holden A J, Robbins D J, Stewart W J. Low frequency plasmons in thin-wire structures. Journal of Physics Condensed Matter, 1998, 10(22): 4785–4809
4. Pendry J B, Holden A J, Robbins D J, Stewart W J. Magnetism from conductors and enhanced nonlinear phenomena. IEEE Transactions on Microwave Theory and Techniques, 1999, 47 (11): 2075–2084
5. Smith D R, Padilla W J, Vier D C, Nemat-Nasser S C, Schultz S. Composite medium with simultaneously negative permeability and permittivity. Physical Review Letters, 2000, 84(18): 4184–4187
6. Shelby R A, Smith D R, Schultz S. Experimental verification of a negative index of refraction. Science, 2001, 292(5514): 77–79
7. Houck A A, Brock J B, Chuang I L. Experimental observations of a left-handed material that obeys Snell's law. Physical Review Letters, 2003, 90(13): 137401
8. Parazzoli C G, Greegor R B, Li K, Koltenbah B E C, Tanielian M. Experimental verification and simulation of negative index of refraction using Snell's law. Physical Review Letters, 2003, 90 (10): 107401
9. Pendry J B. Negative refraction makes a perfect lens. Physical Review Letters, 2000, 85(18): 3966–3969
10. Pendry J B, Ramakrishna S A. Refining the perfect lens. Physica B, Condensed Matter, 2003, 338(1–4): 329–332
11. Fang N, Lee H, Sun C, Zhang X. Sub-diffraction-limited optical imaging with a silver superlens. Science, 2005, 308(5721): 534–537
12. Liu Z, Lee H, Xiong Y, Sun C, Zhang X. Far-field optical hyperlens magnifying sub-diffraction-limited objects. Science, 2007, 315(5819): 1686
13. Leonhardt U. Optical conformal mapping. Science, 2006, 312 (5781): 1777–1780
14. Pendry J B, Schurig D, Smith D R. Controlling electromagnetic fields. Science, 2006, 312(5781): 1780–1782
15. Schurig D, Mock J J, Justice B J, Cummer S A, Pendry J B, Starr A F, Smith D R. Metamaterial electromagnetic cloak at microwave frequencies. Science, 2006, 314(5801): 977–980
16. Engheta N. Thin absorbing screens using metamaterial surfaces. In: Proceedings of IEEE Antennas and Propagation Society International Symposium. San Antonio: IEEE, 2002, 392–395
17. Tretyakov S A, Maslovski S I. Thin absorbing structure for all incidence angles based on the use of a high-impedance surface. Microwave and Optical Technology Letters, 2003, 38(3): 175–178
18. Landy N I, Bingham C M, Tyler T, Jokerst N, Smith D R, Padilla W J. Design, theory, and measurement of a polarization-insensitive absorber for terahertz imaging. Physical Review B, 2009, 79(12): 125104
19. Liu X, Starr T, Starr A F, Padilla W J. Infrared spatial and frequency selective metamaterial with near-unity absorbance. Physical Review Letters, 2010, 104(20): 207403
20. Hao J, Yuan Y, Ran L, Jiang T, Kong J A, Chan C T, Zhou L. Manipulating electromagnetic wave polarizations by anisotropic metamaterials. Physical Review Letters, 2007, 99(6): 063908
21. Zhang S, Park Y S, Li J, Lu X, Zhang W, Zhang X. Negative refractive index in chiral metamaterials. Physical Review Letters, 2009, 102(2): 023901
22. Chen H T, Padilla W J, Cich M J, Azad A K, Averitt R D, Taylor A J. A metamaterial solid-state terahertz phase modulator. Nature Photonics, 2009, 3(3): 148–151
23. Burresi M, Diessel D, van Oosten D, Linden S, Wegener M, Kuipers L. Negative-index metamaterials: looking into the unit cell. Nano Letters, 2010, 10(7): 2480–2483
24. Hsiao H H, Chu C H, Tsai D P. Fundamentals and applications of metasurfaces. Small Methods, 2017, 1(4): 1600064
25. He Q, Sun S, Xiao S, Zhou L. High-efficiency metasurfaces: principles, realizations, and applications. Advanced Optical Materials, 2018, 6(19): 1800415
26. Chen S, Li Z, Zhang Y, Cheng H, Tian J. Phase manipulation of electromagnetic waves with metasurfaces and its applications in

nanophotonics. Advanced Optical Materials, 2018, 6(13): 1800104
27. Hu Y, Wang X, Luo X, Ou X, Li L, Chen Y, Ping Yang, Wang S, Duan H. All-dielectric metasurfaces for polarization manipulation: principles and emerging applications. Nanophotonics, 2020, 9(12): 3755–3780
28. Yu N, Genevet P, Kats M A, Aieta F, Tetienne J P, Capasso F, Gaburro Z. Light propagation with phase discontinuities: generalized laws of reflection and refraction. Science, 2011, 334(6054): 333–337
29. Chen W T, Zhu A Y, Khorasaninejad M, Shi Z, Sanjeev V, Capasso F. Immersion meta-lenses at visible wavelengths for nanoscale imaging. Nano Letters, 2017, 17(5): 3188–3194
30. Tseng M L, Hsiao H H, Chu C H, Chen M K, Sun G, Liu A Q, Tsai D P. Metalenses: advances and applications. Advanced Optical Materials, 2018, 6(18): 1800554
31. Liang H, Martins A, Borges B H V, Zhou J, Martins E R, Li J, Krauss T F. High performance metalenses: numerical aperture, aberrations, chromaticity, and trade-offs. Optica, 2019, 6(12): 1461
32. Moon S W, Kim Y, Yoon G, Rho J. Recent progress on ultrathin metalenses for flat optics. iScience, 2020, 23(12): 101877
33. Zou X, Zheng G, Yuan Q, Zang W, Chen R, Li T, Li L, Wang S, Wang Z, Zhu S. Imaging based on metalenses. PhotoniX, 2020, 1 (1): 2
34. Huang L, Chen X, Mühlenbernd H, Li G, Bai B, Tan Q, Jin G, Zentgraf T, Zhang S. Dispersionless phase discontinuities for controlling light propagation. Nano Letters, 2012, 12(11): 5750–5755
35. Zhou Z, Li J, Su R, Yao B, Fang H, Li K, Zhou L, Liu J, Stellinga D, Reardon C P, Krauss T F, Wang X. Efficient silicon metasurfaces for visible light. ACS Photonics, 2017, 4(3): 544–551
36. Arbabi E, Arbabi A, Kamali S M, Horie Y, Faraon A. Controlling the sign of chromatic dispersion in diffractive optics with dielectric metasurfaces. Optica, 2017, 4(6): 625
37. Lawrence N, Trevino J, Dal Negro L. Aperiodic arrays of active nanopillars for radiation engineering. Journal of Applied Physics, 2012, 111(11): 113101
38. Li X, Xiao S, Cai B, He Q, Cui T J, Zhou L. Flat metasurfaces to focus electromagnetic waves in reflection geometry. Optics Letters, 2012, 37(23): 4940–4942
39. Sun S, He Q, Xiao S, Xu Q, Li X, Zhou L. Gradient-index meta-surfaces as a bridge linking propagating waves and surface waves. Nature Materials, 2012, 11(5): 426–431
40. Sun S, Yang K Y, Wang C M, Juan T K, Chen W T, Liao C Y, He Q, Xiao S, Kung W T, Guo G Y, Zhou L, Tsai D P. High-efficiency broadband anomalous reflection by gradient meta-surfaces. Nano Letters, 2012, 12(12): 6223–6229
41. Walther B, Helgert C, Rockstuhl C, Setzpfandt F, Eilenberger F, Kley E B, Lederer F, Tünnermann A, Pertsch T. Spatial and spectral light shaping with metamaterials. Advanced Materials, 2012, 24(47): 6300–6304
42. Chen W T, Yang K Y, Wang C M, Huang Y W, Sun G, Chiang I D, Liao C Y, Hsu W L, Lin H T, Sun S, Zhou L, Liu A Q, Tsai D P. High-efficiency broadband meta-hologram with polarization-controlled dual images. Nano Letters, 2014, 14(1): 225–230
43. Jiang Z H, Yun S, Lin L, Bossard J A, Werner D H, Mayer T S. Tailoring dispersion for broadband low-loss optical metamaterials using deep-subwavelength Inclusions. Scientific Reports, 2013, 3 (1): 1571
44. Pfeiffer C, Grbic A. Metamaterial Huygens' surfaces: tailoring wave fronts with reflectionless sheets. Physical Review Letters, 2013, 110(19): 197401
45. Yang Y, Wang W, Moitra P, Kravchenko I I, Briggs D P, Valentine J. Dielectric meta-reflectarray for broadband linear polarization conversion and optical vortex generation. Nano Letters, 2014, 14 (3): 1394–1399
46. Yao Y, Shankar R, Kats M A, Song Y, Kong J, Loncar M, Capasso F. Electrically tunable metasurface perfect absorbers for ultrathin mid-infrared optical modulators. Nano Letters, 2014, 14(11): 6526–6532
47. Aieta F, Kats M A, Genevet P, Capasso F. Multiwavelength achromatic metasurfaces by dispersive phase compensation. Science, 2015, 347(6228): 1342–1345
48. Decker M, Staude I, Falkner M, Dominguez J, Neshev D N, Brener I, Pertsch T, Kivshar Y S. High-efficiency dielectric Huygens' surfaces. Advanced Optical Materials, 2015, 3(6): 813–820
49. Zhu W, Song Q, Yan L, Zhang W, Wu P C, Chin L K, Cai H, Tsai D P, Shen Z X, Deng T W, Ting S K, Gu Y, Lo G Q, Kwong D L, Yang Z C, Huang R, Liu A Q, Zheludev N. A flat lens with tunable phase gradient by using random access reconfigurable metamaterial. Advanced Materials, 2015, 27(32): 4739–4743
50. Almeida E, Bitton O, Prior Y. Nonlinear metamaterials for holography. Nature Communications, 2016, 7(1): 12533
51. Almeida E, Shalem G, Prior Y. Subwavelength nonlinear phase control and anomalous phase matching in plasmonic metasurfaces. Nature Communications, 2016, 7(1): 10367
52. Hu J, Zhao X, Lin Y, Zhu A, Zhu X, Guo P, Cao B, Wang C. All-dielectric metasurface circular dichroism waveplate. Scientific Reports, 2017, 7(1): 41893
53. Shitrit N, Bretner I, Gorodetski Y, Kleiner V, Hasman E. Optical spin Hall effects in plasmonic chains. Nano Letters, 2011, 11(5): 2038–2042
54. Chen X, Huang L, Mühlenbernd H, Li G, Bai B, Tan Q, Jin G, Qiu C W, Zhang S, Zentgraf T. Dual-polarity plasmonic metalens for visible light. Nature Communications, 2012, 3(1): 1198
55. Kang M, Chen J, Wang X L, Wang H T. Twisted vector field from an inhomogeneous and anisotropic metamaterial. Journal of the Optical Society of America B, Optical Physics, 2012, 29(4): 572–576
56. Kang M, Feng T, Wang H T, Li J. Wave front engineering from an array of thin aperture antennas. Optics Express, 2012, 20(14): 15882–15890
57. Li G, Kang M, Chen S, Zhang S, Pun E Y, Cheah K W, Li J. Spin-enabled plasmonic metasurfaces for manipulating orbital angular momentum of light. Nano Letters, 2013, 13(9): 4148–4151
58. Lin D, Fan P, Hasman E, Brongersma M L. Dielectric gradient metasurface optical elements. Science, 2014, 345(6194): 298–302
59. Shaltout A, Liu J, Shalaev V M, Kildishev A V. Optically active metasurface with non-chiral plasmonic nanoantennas. Nano Letters, 2014, 14(8): 4426–4431
60. Ding X, Monticone F, Zhang K, Zhang L, Gao D, Burokur S N, de Lustrac A, Wu Q, Qiu C W, Alù A. Ultrathin pancharatnam-berry metasurface with maximal cross-polarization efficiency. Advanced

Materials, 2015, 27(7): 1195–1200
61. Kim J, Li Y, Miskiewicz M N, Oh C, Kudenov M W, Escuti M J. Fabrication of ideal geometric-phase holograms with arbitrary wavefronts. Optica, 2015, 2(11): 958
62. Li G, Chen S, Pholchai N, Reineke B, Wong P W, Pun E Y, Cheah K W, Zentgraf T, Zhang S. Continuous control of the nonlinearity phase for harmonic generations. Nature Materials, 2015, 14(6): 607–612
63. Luo W, Xiao S, He Q, Sun S, Zhou L. Photonic spin hall effect with nearly 100% efficiency. Advanced Optical Materials, 2015, 3 (8): 1102–1108
64. Wen D, Yue F, Li G, Zheng G, Chan K, Chen S, Chen M, Li K F, Wong P W, Cheah K W, Pun E Y, Zhang S, Chen X. Helicity multiplexed broadband metasurface holograms. Nature Communications, 2015, 6(1): 8241
65. Zheng G, Mühlenbernd H, Kenney M, Li G, Zentgraf T, Zhang S. Metasurface holograms reaching 80% efficiency. Nature Nanotechnology, 2015, 10(4): 308–312
66. Ee H S, Agarwal R. Tunable metasurface and flat optical zoom lens on a stretchable substrate. Nano Letters, 2016, 16(4): 2818–2823
67. Khorasaninejad M, Ambrosio A, Kanhaiya P, Capasso F. Broadband and chiral binary dielectric meta-holograms. Science Advances, 2016, 2(5): e1501258
68. Khorasaninejad M, Chen W T, Devlin R C, Oh J, Zhu A Y, Capasso F. Metalenses at visible wavelengths: Diffraction-limited focusing and subwavelength resolution imaging. Science, 2016, 352(6290): 1190–1194
69. Chen W T, Khorasaninejad M, Zhu A Y, Oh J, Devlin R C, Zaidi A, Capasso F. Generation of wavelength-independent subwavelength Bessel beams using metasurfaces. Light, Science & Applications, 2017, 6(5): e16259
70. Luo W, Sun S, Xu H X, He Q, Zhou L. Transmissive ultrathin pancharatnam-berry metasurfaces with nearly 100% efficiency. Physical Review Applied, 2017, 7(4): 044033
71. Ma Z, Li Y, Li Y, Gong Y, Maier S A, Hong M. All-dielectric planar chiral metasurface with gradient geometric phase. Optics Express, 2018, 26(5): 6067–6078
72. Xu R, Chen P, Tang J, Duan W, Ge S J, Ma L L, Wu R X, Hu W, Lu Y Q. Perfect higher-order Poincaré sphere beams from digitalized geometric phases. Physical Review Applied, 2018, 10 (3): 034061
73. Yoon G, Lee D, Nam K T, Rho J. "Crypto-display" in dual-mode metasurfaces by simultaneous control of phase and spectral responses. ACS Nano, 2018, 12(7): 6421–6428
74. Ansari M A, Kim I, Lee D, Waseem M H, Zubair M, Mahmood N, Badloe T, Yerci S, Tauqeer T, Mehmood M Q, Rho J. A spin-encoded all-dielectric metahologram for visible light. Laser & Photonics Reviews, 2019, 13(5): 1900065
75. Xu T, Du C, Wang C, Luo X. Subwavelength imaging by metallic slab lens with nanoslits. Applied Physics Letters, 2007, 91(20): 201501
76. Arbabi A, Horie Y, Ball A J, Bagheri M, Faraon A. Subwavelength-thick lenses with high numerical apertures and large efficiency based on high-contrast transmitarrays. Nature Communications, 2015, 6(1): 7069
77. Khorasaninejad M, Zhu A Y, Roques-Carmes C, Chen W T, Oh J, Mishra I, Devlin R C, Capasso F. Polarization-insensitive metalenses at visible wavelengths. Nano Letters, 2016, 16(11): 7229–7234
78. Sun W, He Q, Sun S, Zhou L. High-efficiency surface plasmon meta-couplers: concept and microwave-regime realizations. Light, Science & Applications, 2016, 5(1): e16003
79. Lalanne P, Astilean S, Chavel P, Cambril E, Launois H. Blazed binary subwavelength gratings with efficiencies larger than those of conventional échelette gratings. Optics Letters, 1998, 23(14): 1081–1083
80. Schonbrun E, Seo K, Crozier K B. Reconfigurable imaging systems using elliptical nanowires. Nano Letters, 2011, 11(10): 4299–4303
81. West P R, Stewart J L, Kildishev A V, Shalaev V M, Shkunov V V, Strohkendl F, Zakharenkov Y A, Dodds R K, Byren R. All-dielectric subwavelength metasurface focusing lens. Optics Express, 2014, 22(21): 26212–26221
82. Zhang Q, Li M, Liao T, Cui X. Design of beam deflector, splitters, wave plates and metalens using photonic elements with dielectric metasurface. Optics Communications, 2018, 411: 93–100
83. Yu N, Aieta F, Genevet P, Kats M A, Gaburro Z, Capasso F. A broadband, background-free quarter-wave plate based on plasmonic metasurfaces. Nano Letters, 2012, 12(12): 6328–6333
84. Yu N, Genevet P, Aieta F, Kats M A, Blanchard R, Aoust G, Tetienne J P, Gaburro Z, Capasso F. Flat optics: controlling wavefronts with optical antenna metasurfaces. IEEE Journal of Selected Topics in Quantum Electronics, 2013, 19(3): 4700423
85. Aieta F, Genevet P, Kats M A, Yu N, Blanchard R, Gaburro Z, Capasso F. Aberration-free ultrathin flat lenses and axicons at telecom wavelengths based on plasmonic metasurfaces. Nano Letters, 2012, 12(9): 4932–4936
86. Ni X, Ishii S, Kildishev A V, Shalaev V M. Ultra-thin, planar, Babinet-inverted plasmonic metalenses. Light, Science & Applications, 2013, 2(4): e72
87. Balthasar Mueller J P, Rubin N A, Devlin R C, Groever B, Capasso F. Metasurface polarization optics: independent phase control of arbitrary orthogonal states of polarization. Physical Review Letters, 2017, 118(11): 113901
88. Wang S, Wu P C, Su V C, Lai Y C, Hung Chu C, Chen J W, Lu S H, Chen J, Xu B, Kuan C H, Li T, Zhu S, Tsai D P. Broadband achromatic optical metasurface devices. Nature Communications, 2017, 8(1): 187
89. Chen W T, Zhu A Y, Sanjeev V, Khorasaninejad M, Shi Z, Lee E, Capasso F. A broadband achromatic metalens for focusing and imaging in the visible. Nature Nanotechnology, 2018, 13(3): 220–226
90. Chen W T, Zhu A Y, Sisler J, Huang Y W, Yousef K M A, Lee E, Qiu C W, Capasso F. Broadband achromatic metasurface-refractive optics. Nano Letters, 2018, 18(12): 7801–7808
91. Li S, Li X, Wang G, Liu S, Zhang L, Zeng C, Wang L, Sun Q, Zhao W, Zhang W. Multidimensional manipulation of photonic spin Hall effect with a single-layer dielectric metasurface. Advanced Optical Materials, 2019, 7(5): 1801365
92. Tian S, Guo H, Hu J, Zhuang S. Dielectric longitudinal bifocal metalens with adjustable intensity and high focusing efficiency. Optics Express, 2019, 27(2): 680–688

93. Chen W T, Török P, Foreman M R, Liao C Y, Tsai W Y, Wu P R, Tsai D P. Integrated plasmonic metasurfaces for spectropolarimetry. Nanotechnology, 2016, 27(22): 224002
94. Yuan Y, Sun S, Chen Y, Zhang K, Ding X, Ratni B, Wu Q, Burokur S N, Qiu C W. A fully phase-modulated metasurface as an energy-controllable circular polarization router. Advanced Science, 2020, 7(18): 2001437
95. Zhang J, Liang Y, Wu S, Xu W, Zheng S, Zhang L. Single-layer dielectric metasurface with giant chiroptical effects combining geometric and propagation phase. Optics Communications, 2021, 478: 126405
96. Arbabi A, Horie Y, Bagheri M, Faraon A. Dielectric metasurfaces for complete control of phase and polarization with subwavelength spatial resolution and high transmission. Nature Nanotechnology, 2015, 10(11): 937–943
97. Arbabi E, Arbabi A, Kamali S M, Horie Y, Faraon A. High efficiency double-wavelength dielectric metasurface lenses with dichroic birefringent meta-atoms. Optics Express, 2016, 24(16): 18468–18477
98. Liu Z, Li Z, Liu Z, Li J, Cheng H, Yu P, Liu W, Tang C, Gu C, Li J, Chen S, Tian J. High-performance broadband circularly polarized beam deflector by mirror effect of multinanorod metasurfaces. Advanced Functional Materials, 2015, 25(34): 5428–5434
99. Nagasaki Y, Suzuki M, Takahara J. All-dielectric dual-color pixel with subwavelength resolution. Nano Letters, 2017, 17(12): 7500–7506
100. Liang H, Lin Q, Xie X, Sun Q, Wang Y, Zhou L, Liu L, Yu X, Zhou J, Krauss T F, Li J. Ultrahigh numerical aperture metalens at visible wavelengths. Nano Letters, 2018, 18(7): 4460–4466
101. Liu C H, Zheng J, Colburn S, Fryett T K, Chen Y, Xu X, Majumdar A. Ultrathin van der Waals metalenses. Nano Letters, 2018, 18(11): 6961–6966
102. Khorasaninejad M, Aieta F, Kanhaiya P, Kats M A, Genevet P, Rousso D, Capasso F. Achromatic metasurface lens at telecommunication wavelengths. Nano Letters, 2015, 15(8): 5358–5362
103. Shi Z, Khorasaninejad M, Huang Y W, Roques-Carmes C, Zhu A Y, Chen W T, Sanjeev V, Ding Z W, Tamagnone M, Chaudhary K, Devlin R C, Qiu C W, Capasso F. Single-layer metasurface with controllable multiwavelength functions. Nano Letters, 2018, 18(4): 2420–2427
104. Shrestha S, Overvig A C, Lu M, Stein A, Yu N. Broadband achromatic dielectric metalenses. Light, Science & Applications, 2018, 7(1): 85
105. Fan Z B, Qiu H Y, Zhang H L, Pang X N, Zhou L D, Liu L, Ren H, Wang Q H, Dong J W. A broadband achromatic metalens array for integral imaging in the visible. Light, Science & Applications, 2019, 8(1): 67
106. Wang S, Wu P C, Su V C, Lai Y C, Chen M K, Kuo H Y, Chen B H, Chen Y H, Huang T T, Wang J H, Lin R M, Kuan C H, Li T, Wang Z, Zhu S, Tsai D P. A broadband achromatic metalens in the visible. Nature Nanotechnology, 2018, 13(3): 227–232
107. Lin R J, Su V C, Wang S, Chen M K, Chung T L, Chen Y H, Kuo H Y, Chen J W, Chen J, Huang Y T, Wang J H, Chu C H, Wu P C, Li T, Wang Z, Zhu S, Tsai D P. Achromatic metalens array for full-colour light-field imaging. Nature Nanotechnology, 2019, 14(3): 227–231
108. Ye M, Ray V, Yi Y S. Achromatic flat subwavelength grating lens over whole visible bandwidths. IEEE Photonics Technology Letters, 2018, 30(10): 955–958
109. Zhang Z, Cui Z, Liu Y, Wang S, Staude I, Yang Z, Zhao M. Design of a broadband achromatic dielectric metalens for linear polarization in the near-infrared spectrum. OSA Continuum, 2018, 1(3): 882–890
110. Chen W T, Zhu A Y, Sisler J, Bharwani Z, Capasso F. A broadband achromatic polarization-insensitive metalens consisting of anisotropic nanostructures. Nature Communications, 2019, 10 (1): 355
111. Cheng Q, Ma M, Yu D, Shen Z, Xie J, Wang J, Xu N, Guo H, Hu W, Wang S, Li T, Zhuang S. Broadband achromatic metalens in terahertz regime. Science Bulletin, 2019, 64(20): 1525–1531
112. Zhao F, Jiang X, Li S, Chen H, Liang G, Wen Z, Zhang Z, Chen G. Optimization-free approach for broadband achromatic metalens of high-numerical-aperture with high-index dielectric metasurface. Journal of Physics D, Applied Physics, 2019, 52(50): 505110
113. Chung H, Miller O D. High-NA achromatic metalenses by inverse design. Optics Express, 2020, 28(5): 6945–6965
114. Ou K, Yu F, Li G, Wang W, Miroshnichenko A E, Huang L, Wang P, Li T, Li Z, Chen X, Lu W. Mid-infrared polarization-controlled broadband achromatic metadevice. Science Advances, 2020, 6 (37): eabc0711
115. Sisler J, Chen WT, Zhu AY, Capasso F. Controlling dispersion in multifunctional metasurfaces. APL Photonics, 2020, 5(5): 056107
116. Zhao F, Li Z, Dai X, Liao X, Li S, Cao J, Shang Z, Zhang Z, Liang G, Chen G, Li H, Wen Z. Broadband achromatic sub-diffraction focusing by an amplitude-modulated terahertz metalens. Advanced Optical Materials, 2020, 8(21): 2000842
117. Yoon G, Kim I, Rho J. Challenges in fabrication towards realization of practical metamaterials. Microelectronic Engineering, 2016, 163: 7–20
118. Zuo R, Liu W, Cheng H, Chen S, Tian J. Breaking the diffraction limit with radially polarized light based on dielectric metalenses. Advanced Optical Materials, 2018, 6(21): 1800795
119. Li Z, Zhang T, Wang Y, Kong W, Zhang J, Huang Y, Wang C, Li X, Pu M, Luo X. Achromatic broadband super-resolution imaging by super-oscillatory metasurface. Laser & Photonics Reviews, 2018, 12(10): 1800064
120. Lin R, Li X. Multifocal metalens based on multilayer Pancharatnam–Berry phase elements architecture. Optics Letters, 2019, 44(11): 2819
121. Gao S, Park C S, Zhou C, Lee S S, Choi D Y. Twofold polarization-selective all-dielectric Trifoci metalens for linearly polarized visible light. Advanced Optical Materials, 2019, 7(21): 1900883
122. Khorasaninejad M, Chen W T, Zhu A Y, Oh J, Devlin R C, Rousso D, Capasso F. Multispectral chiral imaging with a metalens. Nano Letters, 2016, 16(7): 4595–4600
123. Zang X, Ding H, Intaravanne Y, Chen L, Peng Y, Xie J, Ke Q, Balakin A V, Shkurinov A P, Chen X, Zhu Y, Zhuang S. A multi-foci metalens with polarization-rotated focal points. Laser & Photonics Reviews, 2019, 13(12): 1900182
124. Aiello M D, Backer A S, Sapon A J, Smits J, Perreault J D, Llull P, Acosta V M. Achromatic varifocal metalens for the visible

spectrum. ACS Photonics, 2019, 6(10): 2432–2440
125. Arbabi E, Arbabi A, Kamali S M, Horie Y, Faraji-Dana M, Faraon A. MEMS-tunable dielectric metasurface lens. Nature Communications, 2018, 9(1): 812
126. Yilmaz N, Ozdemir A, Ozer A, Kurt H. Rotationally tunable polarization-insensitive single and multifocal metasurface. Journal of Optics, 2019, 21(4): 045105
127. Wei Y, Wang Y, Feng X, Xiao S, Wang Z, Hu T, Hu M, Song J, Wegener M, Zhao M, Xia J, Yang Z. Compact optical polarization-insensitive zoom metalens doublet. Advanced Optical Materials, 2020, 8(13): 2000142
128. Arbabi E, Arbabi A, Kamali S M, Horie Y, Faraon A. Multiwavelength polarization-insensitive lenses based on dielectric metasurfaces with meta-molecules. Optica, 2016, 3(6): 628
129. Kwon H, Arbabi E, Kamali S M, Faraji-Dana M, Faraon A. Single-shot quantitative phase gradient microscopy using a system of multifunctional metasurfaces. Nature Photonics, 2020, 14(2): 109–114
130. Huo P, Zhang C, Zhu W, Liu M, Zhang S, Zhang S, Chen L, Lezec H J, Agrawal A, Lu Y, Xu T. Photonic spin-multiplexing metasurface for switchable spiral phase contrast imaging. Nano Letters, 2020, 20(4): 2791–2798
131. Chen C, Song W, Chen J W, Wang J H, Chen Y H, Xu B, Chen M K, Li H, Fang B, Chen J, Kuo H Y, Wang S, Tsai D P, Zhu S, Li T. Spectral tomographic imaging with aplanatic metalens. Light, Science & Applications, 2019, 8(1): 99
132. Li L, Liu Z, Ren X, Wang S, Su V C, Chen M K, Chu C H, Kuo H Y, Liu B, Zang W, Guo G, Zhang L, Wang Z, Zhu S, Tsai D P. Metalens-array-based high-dimensional and multiphoton quantum source. Science, 2020, 368(6498): 1487–1490

Xiao Fu is a postdoctoral fellow led by Prof. Juntao Li at Sun Yat-sen University, China. She obtained her B.E. degree in Photovoltaic and Renewable Energy from University of New South Wales, Australia, and her Ph.D. degree in the field of perovskite solar cells from Australian National University, Australia. Her research interests are optoelectronic devices, metasurfaces, and fabrication of nanostructures.

Haowen Liang is an associate professor at Sun Yat-sen University, China. He received his Ph.D. degree in the field of optical engineering from Sun Yat-sen University, China. His research interests are advanced imaging and displays achieved by optical field manipulation.

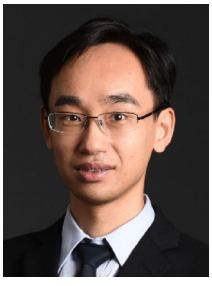

Juntao Li is a professor at Sun Yat-sen University, China. He got his Ph.D. degree in the field of nanophotonic from Sun Yat-sen University, China. His research interests are the photon controlling by the nanophotonic structures.